THE JOURNAL OF PHYSICAL CHEMISTRY LETTERS
A JOURNAL OF THE AMERICAN CHEMICAL SOCIETY

pubs.acs.org/JPCL Letter

# Effects of Methyl Substitution on the Ultrafast Internal Conversion of Benzene

Kazuki Maeda, Alexie Boyer, Shutaro Karashima, Alexander Humeniuk, and Toshinori Suzuki*

Cite This: *J. Phys. Chem. Lett.* 2024, 15, 11760−11766 Read Online



**ABSTRACT:** The effects of methyl substitution on the ultrafast internal conversion from the $S_2(^1B_{1u}, \pi\pi^*)$ state to the $S_0$ state of benzene were studied using ultrafast extreme-ultraviolet photoelectron spectroscopy and electronic structure calculations. The quantum yield of the internal conversion to the $S_0$ state reached ∼0.69 in benzene, while lower values of 0.35 and 0.12 were obtained for toluene and *o*-xylene, respectively. These results indicate that methyl substitution makes the conical intersections less accessible to the nuclear wave packet.

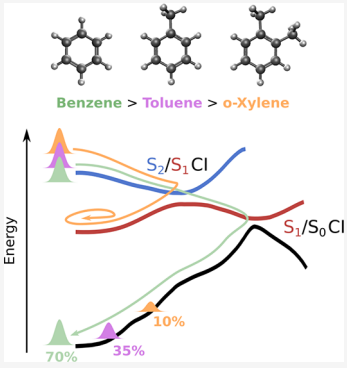


Among the various methods for controlling chemical reactions, the solvent and substituent effects are fundamental. The former influence the reactions through electrostatic interactions or by altering the viscosity of the solvents and are typically utilized in solution chemistry. The latter apply to reactions in the gas phase as well as in solutions. Certain substituents, such as the carbonyl group significantly alter the electronic structure of a molecule by introducing low-lying $^1n\pi^*$ states; similarly, an iodine or bromine atom introduces $^1n\sigma^*$ states. In contrast, methylation of a hydrogen atom in hydrocarbons predominantly impacts vibrational motions with a minor influence on the electronic states. How such a relatively inert methyl group alters molecular dynamics presents an intriguing area of study.[1]

Benzene is the most fundamental aromatic compound and is a cornerstone in the fields of molecular spectroscopy and dynamics. In benzene, the weak $S_1(^1B_{2u}, \pi\pi^*) \leftarrow S_0(^1A_{1g})$ transition starting with a false origin $6_0^1$ at 259 nm is a good example of the intensity borrowing caused by the Herzberg−Teller coupling. The $S_1 \leftarrow S_0$ band exhibits well-resolved vibrational structures and has undergone thorough spectroscopic analysis.[2−6] In contrast, the second ultraviolet (UV) absorption band caused by the $S_2$ $(^1B_{1u}, \pi\pi^*) \leftarrow S_0$ transition starting at ∼205 nm is featureless even at an ultracold temperature,[7] which is attributed to lifetime broadening due to rapid internal conversion.[8−11] Internal conversion is facilitated by conical intersections (CI) among the $S_2/S_1/S_0$ potential energy surfaces, wherein the nuclear wave packet is funneled down to the $S_0$ surface to cause various photochemical reactions.[12−16] Adachi and Suzuki found that ultrafast internal conversion of benzene from the $S_2(^1\pi\pi^*)$ state is altered by methyl substitution; the quantum yield (QY) of $S_0$ decreases in the order 0.92 (benzene) > 0.85 (toluene) > 0.67 (*o*-xylene).[11] This strong methyl substitution effect is of interest. However, the QY estimates based on ground-state bleach recovery measurements were not highly accurate, and theoretical analyses based on electronic structure calculations were lacking.

In this study, extreme UV time-resolved photoelectron spectroscopy (EUV-TRPES) is used to investigate benzene, toluene, and *o*-xylene for their entire relaxation process from the $S_2(^1\pi\pi^*)$ state to the $S_0$ state. The time resolution is ∼38 fs. Unlike the previous study, the branching ratios in the ultrafast internal conversion are estimated by analyzing the photoelectron signal from the individual states of $S_2$, $S_1$ and $S_0$. To analyze the mechanistic details, the potential energy curves are examined using electronic structure calculations at the XMS-CASPT2 (extended multistate complete active space second-order perturbation theory) level of theory. We also performed multiple spawning calculations[17,18] using the CASSCF (complete active space self-consistent field) level of theory are performed to numerically simulate the nonadiabatic transitions.

The experimental apparatus used in this study has been described previously.[19−21] More specifically, a 1 kHz Ti:sapphire regenerative amplifier (35 fs, 800 nm, 6 mJ) was

**Received:** October 1, 2024
**Revised:** November 5, 2024
**Accepted:** November 8, 2024





https://doi.org/10.1021/acs.jpclett.4c02859
*J. Phys. Chem. Lett.* 2024, 15, 11760−11766

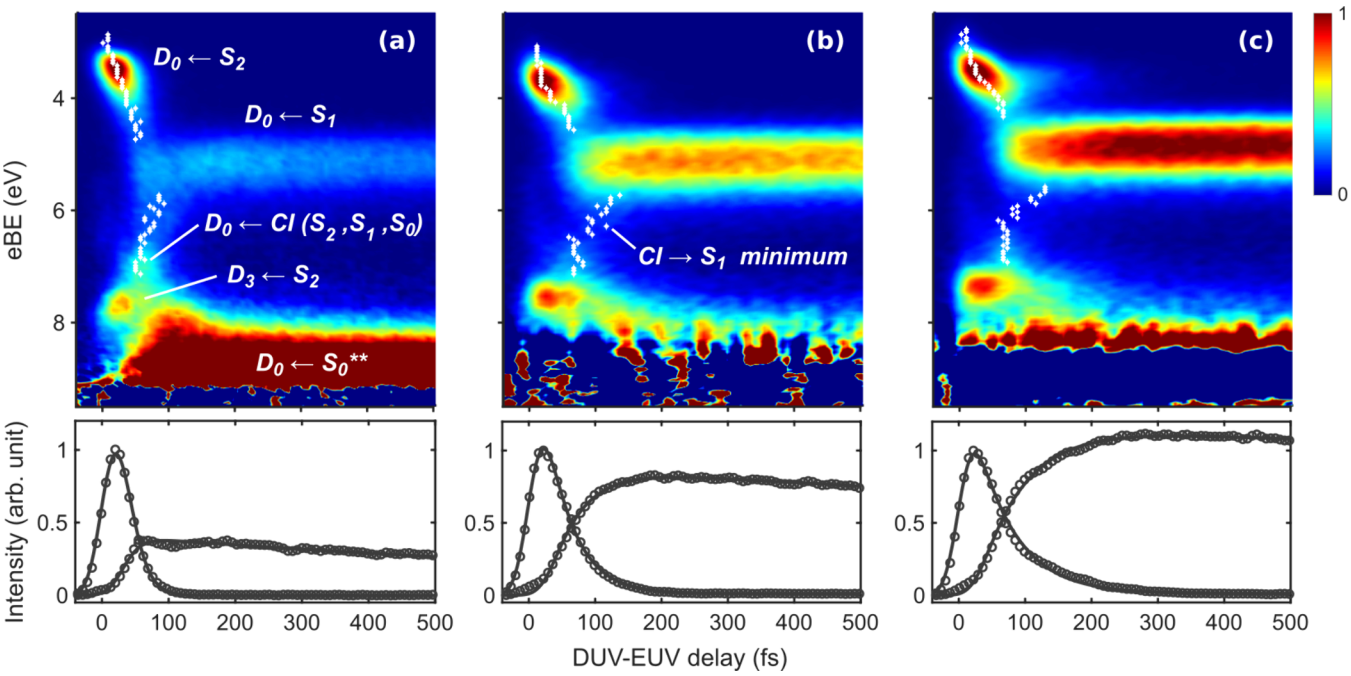


**Figure 1.** TRPE spectra of (a) benzene, (b) toluene, and (c) *o*-xylene. The signal intensities are normalized according to the $D_0 \leftarrow S_2$ PE intensity . The white diamonds indicate the maximum PE intensity for each eBE. The lower panels present the integrated signals (circles) corresponding to $S_2$ decay (2.95−4.1 eV for benzene and *o*-xylene; 3.2−4.35 eV for toluene) and the $S_1$ population (4.65−5.65 eV for benzene; 4.7−5.7 eV for toluene; and 4.4−5.4 eV for *o*-xylene) together with their corresponding fitting curves.

used as the driving laser to produce UV and extreme UV (EUV) radiation. Filamentation four-wave mixing in Ar was used to generate the UV pump pulses (200 nm), whereas high-order harmonic generation in Ar and a time-preserving monochromator[22] were used to generate the EUV probe pulses (21.7 eV). The vapor of the liquid sample at room temperature was seeded in a helium carrier gas, which provided a sample gas concentration of 5% for benzene, and 3% for toluene and *o*-xylene. The molecules were photoexcited using UV pulses and were ionized using time-delayed EUV pulses. The photoelectrons were detected using a magnetic bottle time-of-flight electron energy analyzer.[23] The cross-correlation between the pump and probe pulses was estimated to be ∼38 fs.

The nonadiabatic dynamics following excitation to the $^1\pi\pi^*$ state were simulated using the ab initio multiple spawning (AIMS) method[15,16] implemented in Molpro.[17] Computational settings similar to those used by Toniolo et al.[13] were employed for all molecules. The electronic structure was described using CASSCF with six electrons in five orbitals, averaging over three singlet states. We used the 6-31G* basis set (SA-3-CASSCF(6e,5o)/6-31G*). Initial positions and momenta for 40 individual AIMS runs were sampled from the Wigner distribution in the harmonic potential of the $S_0$ state. Each trajectory commenced in the $S_2$ state and was allowed to propagate for 400 fs with adaptive time stepping and an initial step size of 1 fs. The spawning of further moving basis functions on other electronic states was allowed if (a) the population of the parent trajectory (*PopToSpawn*) was >0.1 and (b) the overlap with the existing basis functions (*OMax*) was <0.6 and (c) the coupling (*CSThresh*) was >0.03. Spawning was disabled after generating a maximum of five trajectories (*MaxTraji*) per run. The adiabatic state populations were obtained by averaging the electronic populations along the trajectories from separate runs.

Figure 1 shows the EUV-TRPE spectra of jet-cooled (a) benzene, (b) toluene, and (c) *o*-xylene, wherein the vertical axis corresponds to the electron binding energy (eBE), given by the difference between the probe photon energy (21.7 eV) and the measured electron kinetic energy (eKE). The one-color one-photon ionization signal of each $S_0$ molecule has already been subtracted. The peak position of the eBE distribution at each time delay corresponds to the vertical electron binding energy (VBE) of the photoexcited nonstationary state. The signal from the Franck−Condon (FC) region in $S_2(^1\pi\pi^*)$ appears at ∼3.5 eV immediately after the photoexcitation. The $S_2(^1\pi\pi^*)$ signal is short-lived for all molecules, and a long-lasting signal appears at ∼5 eV, which originates from the $S_1(^1\pi\pi^*)$ state populated by the ultrafast internal conversion from $S_2$. A comparison of the three PE spectra clearly reveals that the methylation of benzene increases the lifetime of the $S_2$ state, along with the QY of the $S_1$ state, indicating that the internal conversion to the $S_0$ state is hindered by methylation in agreement with the earlier study by Adachi and Suzuki.[11] All molecules show a second photoelectron band at 7.7−7.9 eV, which is due to photoionization from the $S_2$ state to the excited cationic state, $D_3$. The vertical ionization energies from the $S_0$ minima of benzene, toluene, and *o*-xylene are 9.24, 8.82, and 8.56 eV, respectively, indicating that the photoelectron signals in the high eBE regions of the TRPE spectra are obscured by a strong background signal caused by one-photon ionization of the ground-state molecules by the probe pulses. Therefore, the current discussion focuses on values of <9 eV for benzene, and of <8 eV for toluene and *o*-xylene.

The white symbols superimposed on the $S_2(^1\pi\pi^*)$ signal in the figure reveal a rapid shift, indicating nuclear wave packet motion in the $S_2$ state. The rate of change, defined as $d(VBE)/dt$, was found to be −0.030(4) eV/fs for benzene. The white symbols indicated in the 5.5−7.0 eV region initially emerge at


https://doi.org/10.1021/acs.jpclett.4c02859
J. Phys. Chem. Lett. 2024, 15, 11760−11766

~7 eV simultaneously with the disappearance of the $S_2$ signal. Subsequently, they shift from a high to a low eBE, and eventually merge with the strong signal of the $S_1(^1\pi\pi^*)$ state. Based on this spectral feature, the signals indicated by white diamonds in the 5.5−7.0 eV region were attributed to a wave packet motion on the $S_1$ surface prior to relaxation to the global $S_1$ minimum. Since benzene exhibits a significantly larger $S_0$ QY than toluene and *o*-xylene, a clear signature originating from the nonadiabatic transition to $S_0$ should be evident in the spectrum. Indeed, a close examination of the PE spectrum of benzene reveals that the signal at 7 eV is considerably more intense for benzene than for toluene and *o*-xylene; furthermore, a strong signal clearly builds up between 8 and 9 eV in less than 100 fs. These spectral features observed from 7 eV toward a higher eBE value were attributed to the nuclear dynamics of benzene on the $S_0$ surface after the nonadiabatic transition.

Furthermore, the time profiles of the PE signal integrated over the energy ranges of the $S_2$ and $S_1$ states are shown in the bottom panels of Figure 1; the intensities observed for each molecule were normalized to the maximum of the $D_0 \leftarrow S_2$ signal. The decay of the $S_2$ signal can be described by the fitting function

$$I_{S2}(t) = X(t) \otimes \left[U(t-\delta t)A_{S2}\exp\left\{-\frac{t-\delta t}{\tau_{S2}}\right\}\right] \quad (1)$$

where $I(t)$ is the PE intensity, $X(t)$ is the cross-correlation between the pump and probe pulses, $U(x)$ is the Heaviside step function, $\delta t$ is the latency time, $A_{S2}$ is the ionization efficiency of $S_2$, and $\tau_{S2}$ is its decay time. The $S_1$ signal can be described by

$$I_{S1}(t) = X(t) \otimes [U(t-\delta t)\frac{\tau_{S1}}{\tau_{S1}-\tau_{S2}}A_{S1}\left[\exp\left\{-\frac{t-\delta t}{\tau_{S1}}\right\} - \exp\left\{-\frac{t-\delta t}{\tau_{S2}}\right\}\right]] \quad (2)$$

where $A_{S1}$ is the ionization efficiency of $S_1$, and $\tau_{S1}$ is its decay time. Table 1 summarizes the extracted time constants along with previously reported results.[8−10,24−27] The $S_1$ state has a picosecond lifetime, consistent with previous studies. In addition, the three PE spectra reveal that the $S_2$ lifetime and the QY of $S_1$ vary significantly with the methylation of benzene. To estimate the $S_1$ QY from the photoelectron signal intensities of $S_2$ and $S_1$, the $S_2$ and $S_1$ ionization cross sections were estimated from the Dyson norms calculated using XMS-CASPT2; the cross sections were found to be comparable. Thus, we assumed $A_{S2} = A_{S1}$ for eqs 1 and 2. The $S_1$ QY values determined from the photoelectron signals of $S_2$ and $S_1$ were 0.31, 0.65, and 0.88 for benzene, toluene, and *o*-xylene, respectively, as listed in Table 1. This implies that the $S_0$ QY values are 0.69 (0.92), 0.35 (0.85), and 0.12 (0.67) for benzene, toluene, and *o*-xylene, respectively (the numbers in parentheses are taken from the literature[11]). These new results therefore indicate a much greater influence of methylation on the nonadiabatic dynamics of these molecules compared to previous estimates.

**Table 1. Fitting Parameters Extracted Using Eq 1 for the Energy Range of $S_2$ and Eq 2 for the Energy Range of $S_1$**

| | benzene | toluene | *o*-xylene |
|---|---|---|---|
| $\delta t$ (fs) | 30 ± 1 (33)[a] | 20 ± 1 (41)[a] | 17 ± 2 |
| $\tau_{S2}$ (fs) | 16 ± 1 (32)[a] (48)[c] (40)[d] (50)[f] (90)[g] | 41 ± 1 (43)[a] (62)[c] (50)[e] | 59 ± 1 (60)[b] |
| $\tau_{S1}$ (ps) | 1.1[h] (6.7)[f] (5.0)[g] | 3.0[h] (4.3)[e] | 5.8[h] (9.85)[b] |
| $S_1$ QY | 0.31 | 0.65 | 0.88 |
| $As_2/As_1$ | 1.04 | 1.00 | 1.04 |

[a]Reference 24. [b]Reference 25. [c]Reference 10. [d]Reference 8. [e]Reference 26. [f]Reference 9. [g]Reference 27. [h]These values are less accurate than inprevious studies because the measurements were only performed up to 0.6 ps.

Previous measurements of the lifetimes of the $S_2$ state of these molecules using UV-TRPES were less accurate but reasonable. Radloff et al. estimated the lifetimes ($\tau$) of the $S_2$ and $S_1$ states of benzene to be 40 ± 10 fs and 6.7 ± 0.3 ps, respectively.[8,9] A similar study on toluene found $\tau$ of the $S_2$ and $S_1$ states to be 50 ± 10 fs and 4.3 ± 0.2 ps, respectively.[26] For *o*-xylene, Lee et al. reported 60 fs and 9.9 ps for $S_2$ and $S_1$, respectively. Because of the too-narrow pump−probe time window up to 500 fs, our measurements do not provide accurate estimates for the $S_1$ lifetimes; the values in the literature are more accurate. On the other hand, the estimate of QY in UV-TRPES was inaccurate due to insufficient probe photon energy; Radloff et al. initially estimated QY of $S_1$ to be 0.01, which was clearly too low. Stephansen and Sølling have discussed the formation of triplet states,[28] while we found no strong evidence for the generation of the triplet states at least within 200 fs, which is the time scale of the nonadiabatic transition of our interest.

To further extract the details of the ultrafast dynamics in the $S_2$ region (eBE = 3−4.5 eV), the time profile at each eBE was subjected to independent least-squares fitting. The fitting function was similar to eq 1, but with energy dependence

$$I_{S2}(E,t) = X(t) \otimes \left[U(t-\delta t(E))A(E)\exp\left\{-\frac{t-\delta t(E)}{\tau_{S2}(E)}\right\}\right] \quad (3)$$

where $I_{S2}(E,t)$ is the PE intensity, $\delta t(E)$ is the energy-dependent latency time, $A(E)$ is the spectral intensity factor, and $\tau_{S2}(E)$ is the energy-dependent decay time. $\delta t(E)$ is regarded as the arrival time of the nuclear wave packet at the corresponding eBE region, and $\tau_{S2}(E)$ provides a measure for the dispersion of the nuclear wave packet and an inertia effect. A small value of $\tau_{S2}$ indicates that the wave packet motion is ballistic and moves rapidly to the CI, while a large value of $\tau_{S2}$ suggests that the multidimensional wave packet motion occurs along various normal coordinates before it reaches the CI. If the vibrational motion involves a methyl group, the larger inertia increases the propagation time to reach the conical intersection, which can possibly lead to multidimensional vibrational motions and dispersion of the wave packet. Figure 2(a) shows the PE spectrum of *o*-xylene with the VBE values indicated by white diamonds. The rate of change, $d(VBE)/dt$, was calculated to be −0.013(1) eV/fs, which is comparable to that of toluene, while approximately half to that of benzene, i.e., − 0.030(4) eV/fs. In addition, Figures 2(b) and 2(c) show how $\delta t(E)$ and $\tau_{S2}(E)$ vary with the eBE for the three molecules. One can see that the $\delta t(E)$ values are similar for all molecules, while the lifetime $\tau_{S2}(E)$ increases in the order of benzene < toluene < *o*-xylene. The results indicate that the


https://doi.org/10.1021/acs.jpclett.4c02859
J. Phys. Chem. Lett. 2024, 15, 11760−11766

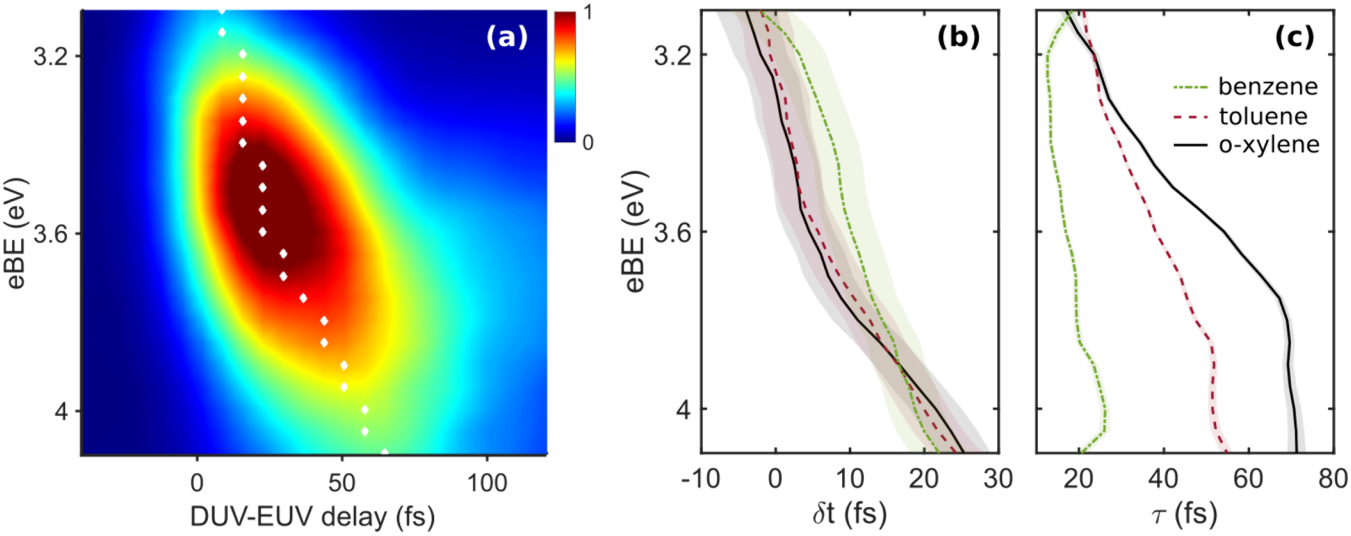


**Figure 2.** (a) TRPE spectrum of *o*-xylene in the $S_2$ region. The white diamonds correspond to the maximum PE intensity at each eBE. The extracted values for (b) $\delta t$ and (c) $\tau$ were obtained using eq 3 for benzene (green), toluene (red), and *o*-xylene (black). The shaded regions in panels (b) and (c) correspond to the standard deviations of the fitting parameters.

nuclear wave packet of benzene is directed more rapidly to the $S_2$−$S_1$ CI located in a ring-puckered geometry (cf., the nuclear wave packets of toluene and *o*-xylene).

To interpret the TRPE spectra, particularly in terms of the methyl substitution effect, electronic structure calculations were performed at the XMS-CASPT2 level of theory. Figure 3 shows the electronic energies of benzene and toluene calculated along the internal conversion pathway. These paths were constructed by geodesical interpolation of the molecular structures between the FC region, the $S_2$−$S_1$ minimum energy conical intersection (MECI), the $S_1$−$S_0$ MECI, and the ground state equilibrium geometry, all of which were optimized at the SA-5-XMS-CASPT2(6e,6o)/cc-pVTZ level of theory. The horizontal axis in this plot is the sum of the lengths of the displacements of all atoms along the path. Based on this plot, it can be predicted that the wave packet starting from the FC region bifurcates after passing through $CI_1$, in which a major part (QY = 0.65) relaxes to $S_0$ through the nearby $S_1$−$S_0$ $CI_2$, and a minor fraction (QY = 0.35) relaxes toward the basin of $S_1$ in the planar geometry. Figures 3(c) and 3(d) show the variations in VBE along the reaction path. Notably, the electronic energy diminishes from $CI_1$ to the planar structure in $S_1$, reproducing the experimental results shown in Figure 1. Considering the path toward $S_0$, the VBE at $CI_2$ was computationally predicted to be ∼7 eV. As mentioned earlier, Figure 1 shows a strong signal at ∼7 eV for benzene, which is attributed to the PE signal from the $CI_2$ region. Figure 1 also reveals the presence of a weak signal that shifts from 7 to 5.5 eV; the peaks of the time profiles measured in this region are indicated by white diamonds in Figure 1. The weak signal moving toward a lower eBE value was ascribed to a part of the wave packet that passes $CI_2$ without relaxing to $S_0$ and remains in $S_1$; this fraction of the signal is rather small. The PE signals at 5.5 and 7 eV appear almost simultaneously, indicating that the wave packet reaches $CI_1$ and $CI_2$ with only a short time lag. Previous computational simulations by Thompson and Martínez[16] indicated that the $S_1$ and $S_0$ populations begin to increase at almost the same time, although $S_1$ increases slightly earlier than $S_0$ (i.e., by ∼10 fs).

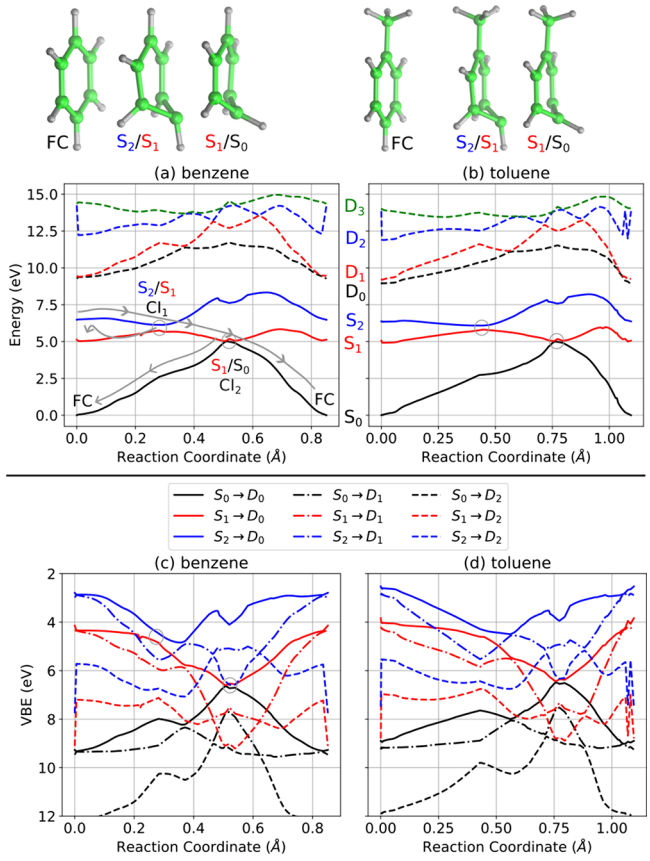


**Figure 3.** Top panels: Potential energy of the lowest neutral and cationic states (computed using SA-5-XMS-CASPT2(6e,12o)/cc-pVTZ) along the reaction path leading from FC point through the $S_2$/$S_1$ and $S_1$/$S_0$ MECIs back to the ground state minimum, (a) for benzene and (b) for toluene. Bottom panels: Vertical electron binding energies along the same path, (c) for benzene and (d) for toluene.

Recently, Robinson et al. analyzed the $S_1$−$S_0$ transition of toluene in terms of the oscillator strength, which depends on the vibronic coupling between the $S_2$ and $S_1$ states.[29] They indicated that the $S_2$/$S_1$ MECI structure of toluene occurs at a


https://doi.org/10.1021/acs.jpclett.4c02859
J. Phys. Chem. Lett. 2024, 15, 11760−11766

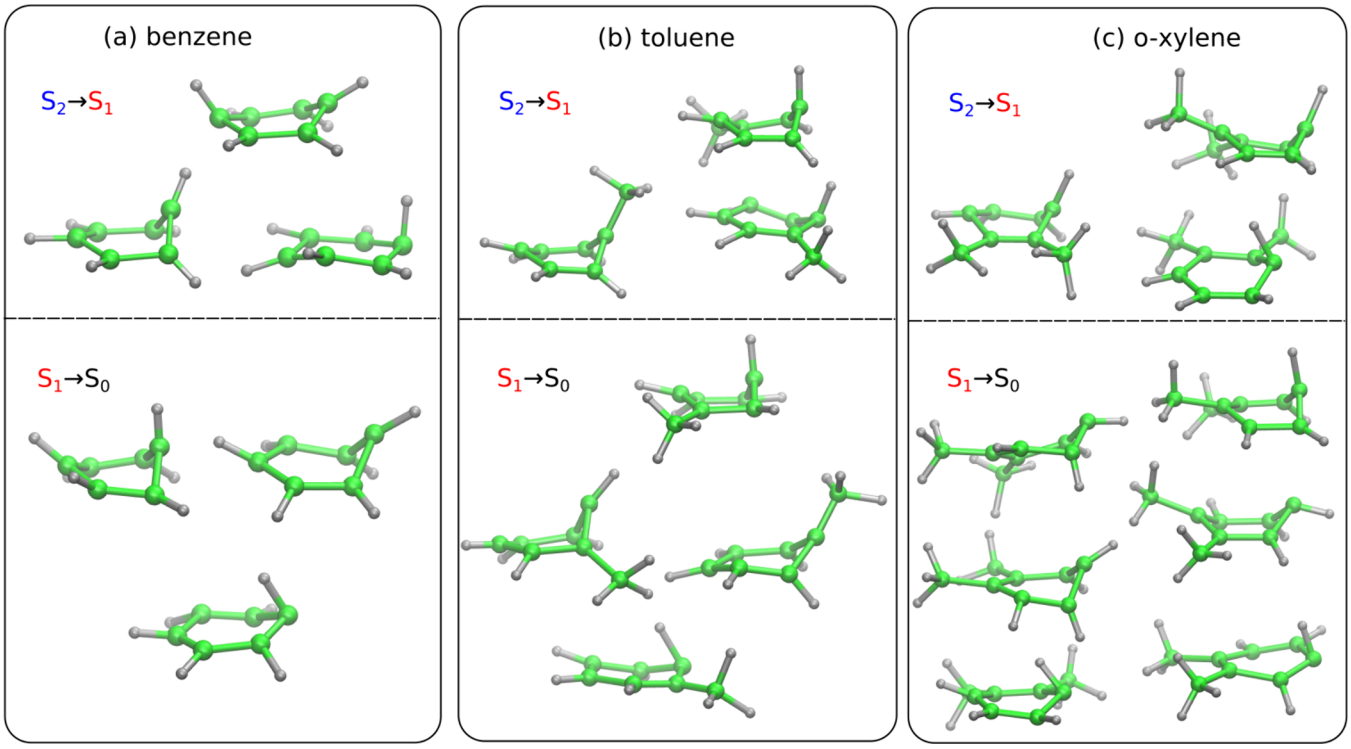


**Figure 4.** Representative geometries at which new trajectory basis functions are spawned due to strong nonadiabatic coupling for (a) benzene, (b) toluene and (c) *o*-xylene.

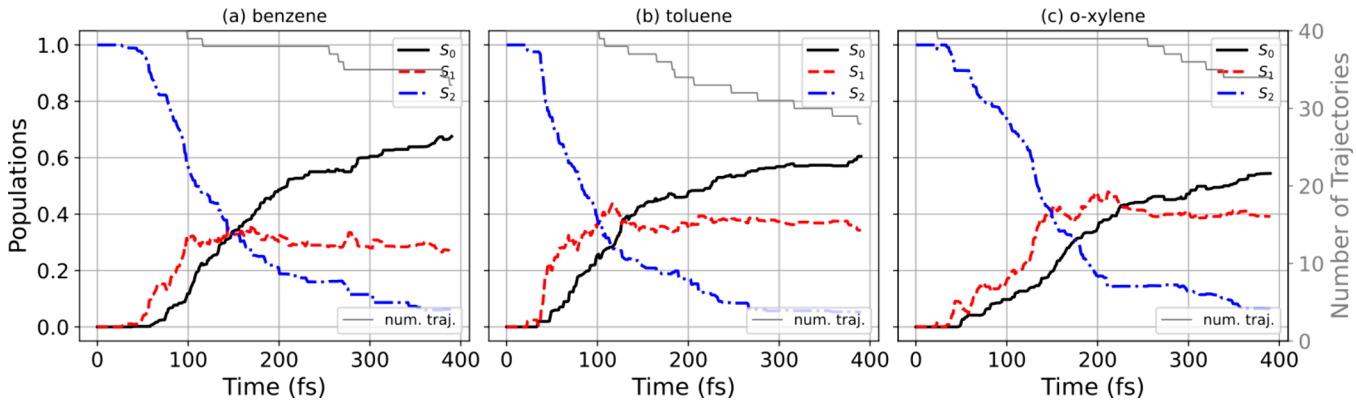


**Figure 5.** Adiabatic state populations determined from the AIMS simulations performed for (a) benzene, (b) toluene, and (c) *o*-xylene. The thin gray line indicates the number of trajectory runs available for averaging at each time step.

puckered structure, with the $CH_3$ group lifted from the molecular plane. We examined the path related to the $S_2 \rightarrow S_1$ and $S_1 \rightarrow S_0$ internal conversions to understand why methyl substitution hinders the latter process. Electronic structure calculations indicated that methyl substitution did not significantly alter the potential energy surfaces. As shown in Figure 3(b), the methyl substituent has no impact on the energetics of $S_2/S_1$ or the geometry of the $S_1/S_0$ CI induced by ring puckering in the *para* position with respect to the methyl group. We also investigated CI that occurs by puckering at the methyl-substituted carbon atom, and it was observed to exhibit only a small change in the energy relative to the CI of benzene. In fact, AIMS calculations revealed that CIs can occur by puckering at various carbon atoms (see Figure 4). However, although the CI energies were similar, the nuclear motions of the methyl-substituted benzenes were inevitably slowed down depending on the degree of motion of the methyl group. In benzene, six symmetry-equivalent CIs are caused by the out-of-plane motion of a single carbon atom, and the wave packet accesses these intersections equally. As mentioned earlier, methyl substitution does not alter the energetics of the CI; however, the motion of the carbon atom becomes slower with methyl substitution. In other words, the topography of the potential energy surface with the mass-weighted coordinates changed with the methyl substitution. More specifically, a greater number of methyl substituents led to slower out-of-plane motion. This explains the increase in the excited-state lifetimes observed in the experimental TRPES of the benzene < toluene < *o*-xylene series. AIMS simulations partially corroborate this interpretation. The recovery of the $S_0$ state population is slowed down and the yield of the $S_1$ state increases with the number of methyl groups. However, the trend is much less pronounced compared to the experimental results (see Figure 5). The dynamic simulation using CASSCF-


https://doi.org/10.1021/acs.jpclett.4c02859
J. Phys. Chem. Lett. 2024, 15, 11760−11766

level quantum chemical calculations qualitatively reproduced the suppression of internal conversion by the methyl group, but yielded insufficient quantitative results. In this study, it was not feasible to perform dynamic calculations considering electron correlation due to computational cost constraints. However, we believe that incorporating dynamic electron correlation in future studies will likely improve the agreement with experimental observations.

In summary, EUV-TRPES was performed on benzene, toluene, and *o*-xylene with a time resolution of 38 fs, and the obtained results were compared with electronic structure calculations carried out at the XMS-CASPT2 level of theory, along with multiple spawning calculations. The nuclear wave packet created in the $S_2$ ($^1B_{1u}$, $\pi\pi^*$) state was found to reach the $S_2$−$S_1$ MECI ∼ 30 fs before bifurcation. It was found that a major fraction of the $S_2$ state relaxes to the $S_0$ state through the nearby $S_1$−$S_0$ MECI, while a minor fraction relaxes toward $S_1$. The relaxation time of the $S_2$ state in benzene was estimated to be ∼16 fs, and the calculations performed herein demonstrated that the energetics of the potential energy surfaces are not affected by methyl substitution. However, the nuclear motions involved in the internal conversion of methyl-substituted benzenes became slower due to the inertia effect, resulting in slower relaxation dynamics of the $S_2$ state, and a higher QY for the $S_1$ state, in the order of benzene < toluene < *o*-xylene.

## ■ ASSOCIATED CONTENT

### Supporting Information

The Supporting Information is available free of charge at https://pubs.acs.org/doi/10.1021/acs.jpclett.4c02859.

Transparent Peer Review report available (PDF)

## ■ AUTHOR INFORMATION


### Corresponding Author

**Toshinori Suzuki** − *Department of Chemistry, Graduate School of Science, Kyoto University, Kyoto 606-8502, Japan;* orcid.org/0000-0002-4603-9168; Email: suzuki.toshinori.2n@kyoto-u.ac.jp

### Authors

**Kazuki Maeda** − *Department of Chemistry, Graduate School of Science, Kyoto University, Kyoto 606-8502, Japan*

**Alexie Boyer** − *Department of Chemistry, Graduate School of Science, Kyoto University, Kyoto 606-8502, Japan;* orcid.org/0000-0003-0838-0573

**Shutaro Karashima** − *Department of Chemistry, Graduate School of Science, Kyoto University, Kyoto 606-8502, Japan*

**Alexander Humeniuk** − *Department of Chemistry, Graduate School of Science, Kyoto University, Kyoto 606-8502, Japan;* orcid.org/0000-0002-3748-4921

Complete contact information is available at: https://pubs.acs.org/10.1021/acs.jpclett.4c02859


### Notes

The authors declare no competing financial interest.

## ■ ACKNOWLEDGMENTS

This study was supported by JSPS KAKENHI Grant No. 21H04970. A.B. thanks the Japan Society for the Promotion of Science for a postdoctoral fellowship. Calculations were performed with the supercomputer system of the Academic Center for Computing and Media Studies at Kyoto University.

## ■ REFERENCES


(1) Schuurman, M. S.; Stolow, A. Dynamics at Conical Intersections. *Annu. Rev. Phys. Chem.* **2018**, *69*, 427−450.

(2) Stephenson, T. A.; Radloff, P. L.; Rice, S. A. $^1B_{2u} \leftrightarrow {}^1A_{1g}$ Spectroscopy of Jet-Cooled Benzene: Single Vibronic Level Fluorescence Studies. *J. Chem. Phys.* **1984**, *81*, 1060−1072.

(3) Stephenson, T. A.; Rice, S. A. Vibrational State Dependence of Radiationless Processes in $^1B_{2u}$ Benzene. *J. Chem. Phys.* **1984**, *81*, 1073−1082.

(4) Parmenter, C. S.; Atkinson, G. H. Absorption Spectrum of Benzene Vapor Near 2537 Ang. *J. Phys. Chem.* **1971**, *75*, 1564−1572.

(5) Knight, A. E. W.; Parmenter, C. S.; Schuyler, M. W. Extended View of the Benzene 260-nm Transition via Single Vibronic Level Fluorescence. I. General Aspects of Benzene Single Vibronic Level Fluorescence. *J. Am. Chem. Soc.* **1975**, *97*, 1993−2005.

(6) Beck, S. M.; Liverman, M. G.; Monts, D. L.; Smalley, R. E. Rotational Analysis of the $^1B_{2u}$ ($\pi\pi$) $\leftarrow {}^1A_{1g}$, ($6^1$) Band of Benzene and Helium−Benzene Van Der Waals Complexes in a Supersonic Jet. *J. Chem. Phys.* **1979**, *70*, 232−237.

(7) Hiraya, A.; Shobatake, K. Direct Absorption Spectra of Jet-Cooled Benzene in 130−260 nm. *J. Chem. Phys.* **1991**, *94*, 7700−7706.

(8) Radloff, W.; Freudenberg, T.; Ritze, H. H.; Stert, V.; Noack, F.; Hertel, I. V. Lifetime of the Benzene Dimer in the $S_2$ Electronic State. *Chem. Phys. Lett.* **1996**, *261*, 301−306.

(9) Radloff, W.; Stert, V.; Freudenberg, T.; Hertel, I. V.; Jouvet, C.; Dedonder-Lardeux, C.; Solgadi, D. Internal Conversion in Highly Excited Benzene and Benzene Dimer: Femtosecond Time-Resolved Photoelectron Spectroscopy. *Chem. Phys. Lett.* **1997**, *281*, 20−26.

(10) Suzuki, Y.-I.; Horio, T.; Fuji, T.; Suzuki, T. Time-Resolved Photoelectron Imaging of $S_2 \rightarrow S_1$ Internal Conversion in Benzene and Toluene. *J. Chem. Phys.* **2011**, *134*, 184313.

(11) Adachi, S.; Suzuki, T. Methyl Substitution Effects on the Non-Adiabatic Dynamics of Benzene: Lifting Three-State Quasi-Degeneracy at Conical Intersections. *Phys. Chem. Chem. Phys.* **2020**, *22*, 2814−2818.

(12) Palmer, I. J.; Ragazos, I. N.; Bernardi, F.; Olivucci, M.; Robb, M. A. An MC-SCF Study of the $S_1$ and $S_2$ Photochemical Reactions of Benzene. *J. Am. Chem. Soc.* **1993**, *115*, 673−682.

(13) Toniolo, A.; Thompson, A. L.; Martínez, T. J. Excited State Direct Dynamics of Benzene with Reparameterized Multi-Reference Semiempirical Configuration Interaction Methods. *Chem. Phys.* **2004**, *304*, 133−145.

(14) Sobolewski, A. L.; Woywod, C.; Domcke, W. *Ab Initio* Investigation of Potential-Energy Surfaces Involved in the Photophysics of Benzene and Pyrazine. *J. Chem. Phys.* **1993**, *98*, 5627−5641.

(15) Hertel, I. V.; Radloff, W. Ultrafast Dynamics in Isolated Molecules and Molecular Clusters. *Rep. Prog. Phys.* **2006**, *69*, 1897−2003.

(16) Thompson, A. L.; Martínez, T. J. Time-Resolved Photoelectron Spectroscopy from First Principles: Excited State Dynamics of Benzene. *Faraday Discuss.* **2011**, *150*, 293.

(17) Ben-Nun, M.; Martínez, T. J. *Ab Initio* Molecular Dynamics Study of *Cis*−*Trans* Photoisomerization in Ethylene. *Chem. Phys. Lett.* **1998**, *298*, 57−65.

(18) Curchod, B. F. E.; Martínez, T. J. *Ab Initio* Nonadiabatic Quantum Molecular Dynamics. *Chem. Rev.* **2018**, *118*, 3305−3336.

(19) Karashima, S.; Humeniuk, A.; Uenishi, R.; Horio, T.; Kanno, M.; Ohta, T.; Nishitani, J.; Mitrić, R.; Suzuki, T. Ultrafast Ring-Opening Reaction of 1,3-Cyclohexadiene: Identification of Non-adiabatic Pathway via Doubly Excited State. *J. Am. Chem. Soc.* **2021**, *143*, 8034−8045.

(20) Miura, Y.; Yamamoto, Y.-i.; Karashima, S.; Orimo, N.; Hara, A.; Fukuoka, K.; Ishiyama, T.; Suzuki, T. Formation of Long-Lived Dark States During Electronic Relaxation of Pyrimidine Nucleobases Studied Using Extreme Ultraviolet Time-Resolved Photoelectron Spectroscopy. *J. Am. Chem. Soc.* **2023**, *145*, 3369−3381.

(21) Karashima, S.; Miao, X.; Kanayama, A.; Yamamoto, Y.-i.; Nishitani, J.; Kavka, N.; Mitrić, R.; Suzuki, T. Ultrafast Ring Closure

Reaction of Gaseous *cis*-Stilbene from $S_1$ ($\pi\pi^*$). *J. Am. Chem. Soc.* **2023**, *145*, 3283−3288.
(22) Frassetto, F.; Cacho, C.; Froud, C. A.; Turcu, I. C. E.; Villoresi, P.; Bryan, W. A.; Springate, E.; Poletto, L. Single-Grating Monochromator for Extreme-Ultraviolet Ultrashort Pulses. *Opt. Express* **2011**, *19*, 19169.
(23) Kurahashi, N.; Thürmer, S.; Liu, S. Y.; Yamamoto, Y.-i.; Karashima, S.; Bhattacharya, A.; Ogi, Y.; Horio, T.; Suzuki, T. Design and Characterization of a Magnetic Bottle Electron Spectrometer for Time-Resolved Extreme UV and X-Ray Photoemission Spectroscopy of Liquid Microjets. *Struct. Dyn.* **2021**, *8*, 034303.
(24) Suzuki, T. Time-Resolved Photoelectron Spectroscopy of Non-Adiabatic Electronic Dynamics in Gas and Liquid Phases. *Int. Rev. Phys. Chem.* **2012**, *31*, 265−318.
(25) Liu, Y.; Tang, B.; Shen, H.; Zhang, S.; Zhang, B. Probing Ultrafast Internal Conversion of o-Xylene via Femtosecond Time-Resolved Photoelectron Imaging. *Opt. Express* **2010**, *18*, 5791.
(26) Farmanara, P.; Stert, V.; Radloff, W.; Hertel, I. V. Ultrafast Internal Conversion in Highly Excited Toluene Monomers and Dimers. *J. Phys. Chem. A* **2001**, *105*, 5613−5617.
(27) Shen, H.; Zhang, B. Ultrafast Dynamics of Benzene on the $S_2$ State Investigated by Femtosecond Time-Resolved Photoelectron Spectroscopy. *Acta Phys. Chim. Sin.* **2015**, *31*, 1662−1666.
(28) Stephansen, A. B.; Sølling, T. I. Distortion Dependent Intersystem Crossing: A Femtosecond Time-Resolved Photoelectron Spectroscopy Study of Benzene, Toluene, and p-Xylene. *Struct. Dyn.* **2017**, *4*, 044008.
(29) Robinson, D.; Alarfaji, S. S.; Hirst, J. D. Benzene, Toluene, and Monosubstituted Derivatives: Diabatic Nature of the Oscillator Strengths of $S_1 \leftarrow S_0$ Transitions. *J. Phys. Chem. A* **2021**, *125*, 5237−5245.


https://doi.org/10.1021/acs.jpclett.4c02859
*J. Phys. Chem. Lett.* 2024, 15, 11760−11766